

Effect of measurement uncertainties on strain-based damage diagnostics for highway bridges

Matthew J. Whelan¹ · Michael V. Gangone²

Received: 5 December 2014 / Revised: 23 March 2015 / Accepted: 25 March 2015
© Springer-Verlag Berlin Heidelberg 2015

Abstract Diagnostic load rating of highway bridges using distributed strain transducers is one of the more prominent strategies applied for both periodic and continuous monitoring of highway bridges. Techniques for load rating structures using experimental measurements of neutral axis locations, girder distribution factors, and dynamic increase factors have been suggested for structural health monitoring and damage detection applications. However, practical considerations related to the influence of measurement uncertainties on the reliability of these diagnostic measures in the presence of damage have only been examined recently. This paper extends uncertainty propagation formulae previously derived for neutral axis measurements to girder distribution factors. The significance of measurement uncertainties on damage-sensitive features are then explored using experimental data from a real bridge subjected to progressive, prescribed damage. The experimental results suggest that both apparent neutral axis locations and girder distribution factors exhibit sensitivity to the damage mechanisms introduced that exceeds the measurement uncertainty. In addition, girder distribution factors are found to demonstrate the ability to locate the damage. Comparisons with finite element simulations underline the challenges associated with faithfully modeling the effects of structural damage and

emphasize the need for continued full-scale validation of structural health monitoring approaches on real structures.

Keywords Load rating · Strain measurement · Measurement uncertainty · Full-scale bridge testing · Damage detection

1 Introduction

Load testing and rating using strain transducers and calibrated test vehicles are often performed by state transportation agencies or independent consulting companies working on behalf of the bridge owner. The process of load testing involves measuring the structural response at critical locations across the bridge under predetermined load patterns applied by known axle weights. Positioning of the test vehicles is prescribed to generate elastic strains of measurable amplitude for each girder of the cross-section. Neutral axis locations, transverse load distribution factors, and dynamic increase factors are computed from the test data and calibrated within analytical models used for inventory and operating load rating calculations to improve the accuracy of the ratings [1]. However, this method, while effective, has to date been applied to only a very small fraction of in-service bridges and only recently has the influence of measurement uncertainties on the reliability of the results been examined.

Through experimental load testing, bridge owners can alleviate network level maintenance, rehabilitation, and repair needs by increasing the often overly conservative load postings developed by purely analytical methods. As evidence of this opportunity, Bakht and Jaeger [2] presented findings from multiple tests conducted in Ontario, Canada of concrete deck on steel girder bridges as well as

✉ Matthew J. Whelan
mwhelan3@uncc.edu

¹ Department of Civil and Environmental Engineering,
University of North Carolina at Charlotte, Charlotte, NC,
USA

² Department of Civil Engineering, University of Texas at
Tyler, Tyler, TX, USA

steel truss bridges. They showed that analytically predicted bridge capacity is often significantly over-conservative compared to experimental results, as distribution factors and neutral axis estimates often differed significantly from the values derived from elementary mechanics. A specific illustrative example was provided wherein a truss bridge posted for 2 metric tons actually carried a static proof load of 70 metric ton. One reason for these differences is the contributions to structural stiffness offered by secondary elements that are often neglected in the analytical predictions, such as the wearing surface and parapets. Burdet [3] discussed the specific effects of secondary bridge components to the stiffness of post-tensioned concrete bridges and found that, while the majority of the stiffness can be attributed to the structural concrete, a significant additional contribution was present from secondary elements. Pressley et al. [4] showed that for flat slab bridges supported by piles, pure bending analysis for capacity estimation was close to the experimental results; however, punching shear affects were not accurately predicted. For each of the three bridges examined in the study, the author references the importance of experimental load rating for accurately determining the load capacity of the bridge.

As an extension of experimental load rating of bridges, the strain-based measurements of neutral axis locations and girder distribution factors have also been proposed for continuous and periodic structural health monitoring. Ni et al. [5] numerically and experimentally investigated using the neutral axis as a damage index for bridge decks using a Kalman filter estimator. The results indicated that the neutral axis is highly sensitive to damage in bridge decks and that the damage can be located in densely instrumented areas. Sigurdardottir and Glisic [6] analyzed the reliability of the neutral axis as a damage indicator from experimental strain measurements by developing a measure of uncertainty based on the measurement error of the sensor system. The authors concluded that apparent neutral axis measurements have the potential to be used as a damage indicator if sufficient statistical data is available to alleviate the effect of measurement uncertainties.

In addition to neutral axis monitoring, changes in girder distribution factors have also been proposed within several studies as a means for structural diagnostics. Finite element simulations were performed in Plude [7] across several representative scenarios of fatigue cracking, loss of composite behavior, and deck deterioration to explore the use of strain-based measurements for damage detection. With the exception of the case of deck deterioration, neutral axis and girder distribution factors were found to be sensitive to simulated cases of damage, although the sensitivity was strongly related to the proximity of the measurement to the location of the damage. As with use of the neutral axis as a damage-sensitive feature, a challenge associated with

diagnostic monitoring using girder distribution factors is that measurement uncertainties affect the repeatability of the girder distribution factor estimates, even if using a calibrated truck load [8]. Recognizing the influence of uncertainties produced by measurement noise and load positioning error, Cardini and DeWolf [9] have suggested using statistical properties of measured distribution factors to envelope the range of expected values. These envelopes are proposed as a means of identifying outliers that are suggestive of the onset of damage. An extension of this envelope-based approach is explored in Reiff [10] by application to numerically generated data. The author concluded through successful application of a damage index to several simulated cases of damage that girder distribution factors are “a robust indicator of bridge performance and potential damage”.

This paper discusses the sensitivity of the neutral axis and distribution factor estimates to measurement uncertainty and is the first to examine the impact of these uncertainties using actual experimental data from full-scale bridge testing. Experimental results from an instrumented simply supported multi-girder bridge span subjected to prescribed, progressive damage are presented alongside numerical predictions to examine the sensitivity of the apparent neutral axis locations and girder distribution factors to the introduced damage in the presence of measurement uncertainty. The results are significant towards identifying appropriate strategies for strain-based structural health monitoring of the prevalent multi-girder bridge design with practical consideration given to measurement errors and other uncertainties that might affect the reliability of the damage-sensitive strain features.

2 Uncertainty propagation analysis

A primary contribution of the current work is to examine how measurement uncertainties affect structural property estimates, particularly when used for diagnosis of damage. Measurement uncertainties arise from numerous random and systematic errors and propagate through subsequent equations used to derive engineering measurands, such as apparent neutral axis location or distribution factors. There are two primary means of evaluating uncertainties, which are classified as Type A or Type B evaluations. A Type A evaluation uses the experimentally measured standard deviation during a period where conditions of measurement are held constant to characterize uncertainties due to random error and precision limitations. In contrast, Type B evaluation uses information such as manufacturer specifications and calibration certificates to estimate uncertainties, which may include additional errors not accounted for in Type A evaluation such as transducer accuracy. When

the Type A and Type B evaluations account for different sources of uncertainty, they can be combined to express the uncertainty due to multiple effects [11].

In the case of the strain measurements used in this paper, it is assumed that uncertainties arise primarily from (1) random errors associated with the precision and repeatability of the instrumentation and (2) systematic errors associated with the accuracy of the transducer. The first can be characterized by Type A evaluation using the experimental standard deviation and are assumed to be independent of strain amplitude. The second can be characterized by Type B evaluation using manufacturer specifications or calibration certificates and are assumed proportional to the amplitude of the measured strain. The relationship between the strain amplitude and these uncertainties as well as their combined standard uncertainty, are presented in Fig. 1. As can be seen, the combined standard uncertainty within measured mechanical strains with relatively low magnitudes will be governed by the transducer precision, while the combined standard uncertainty in measured mechanical strains of high magnitude will be driven by the transducer accuracy. Formulae for evaluating the propagation of these uncertainties through the standard equations used to relate the strain measurements to neutral axis locations and distribution factors are presented in the following subsections.

2.1 Neutral axis

The precision and accuracy of the strain measurements used for estimating in-service neutral axis locations from experimental measurements are very important when using these estimates for experimental load rating and when considering the neutral axis as a diagnostic indicator of damage. Although four transducer arrangements can be employed to compensate for biaxial bending strains, the most commonly used approach for estimating neutral axis locations relies on placement of two transducers at different elevations in the cross-section [12], as shown in Fig. 2a.

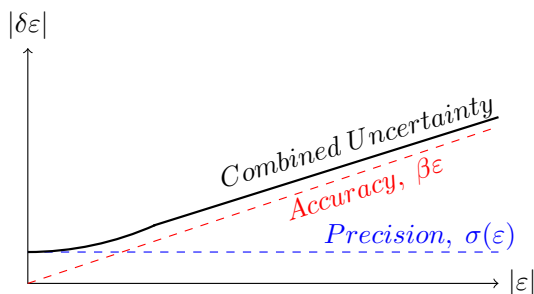


Fig. 1 Uncertainty in strain measurements associated with precision and accuracy, as well as their combined standard uncertainty

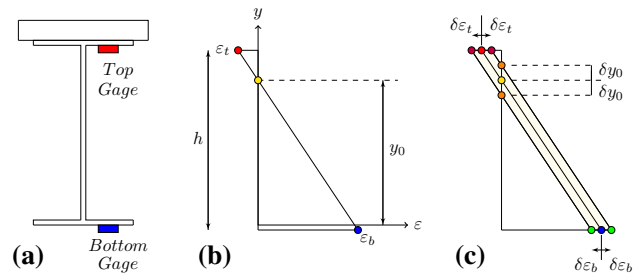


Fig. 2 Typical neutral axis measurement using pair of strain transducers. a Gage placement in the cross-section; b estimation of neutral axis location from linear strain assumption; c effect of measurement uncertainties on accuracy of neutral axis determination

A linear strain distribution is then assumed in the cross-section, which permits the neutral axis to be estimated from the two point measurements of normal strain. However, since both the mechanical strain measurement at the top and the bottom of the cross-section are plagued by measurement uncertainty, the estimation should also be provided with uncertainty bounds.

Few studies have considered the influence of measurement uncertainty on neutral axis measurements; however, Sigurdardottir and Glisic recently developed an uncertainty estimate for the neutral axis measurand by applying the propagation formula. The standard uncertainty in the neutral axis determination (δy_0) was shown to be dependent on the top and bottom strains and the distance separating the strain gages in the cross-section (h). The standard uncertainty was developed by Sigurdardottir and Glisic as [6]:

$$\delta y_0 = \frac{h}{(\epsilon_b - \epsilon_t)^2} [|\epsilon_b| \delta \epsilon_t + |\epsilon_t| \delta \epsilon_b] \quad (1)$$

where ϵ_b and ϵ_t are the measured strains at the bottom and top of the cross-section, respectively, and $\delta \epsilon_b$ and $\delta \epsilon_t$ are the uncertainties associated with these measurements. In the cited article, the authors assumed that uncertainties in the measured mechanical strains are uniform for all sensors in the monitoring system ($\delta \epsilon_t = \delta \epsilon_b = \sigma(\epsilon)$). This estimate can be developed through a Type A evaluation of standard uncertainty by determining the experimental standard deviation of the mean, $\sigma(\epsilon)$. This measure is generally suitable for accounting for uncertainties attributable to random error and measurement precision. Applying the assumption of uniform uncertainty, one can determine the Type A standard uncertainty on the neutral axis measurand using:

$$\delta y_0^A = \frac{(1 + |c|)}{(1 - c)^2} \frac{1}{\epsilon_b} h \sigma(\epsilon) \quad (2)$$

where c is defined as the ratio of the measured strain at the top gage to the measured strain in the bottom gage, ϵ_t/ϵ_b . However, this uncertainty estimate only accounts for the

Type A standard uncertainties and not for additional systematic errors, such as the manufacturer specified accuracy of the calibration. Accounting for such additional uncertainties requires a Type B evaluation of standard uncertainty. In the case of transducer accuracy, which is typically provided as a percentage of the gage factor for strain transducers, the Type B standard uncertainty can be taken as $\delta \varepsilon_k = \beta |\varepsilon_k|$, where β is the accuracy of the transducer calibration. Assuming all transducers have the same stated accuracy, the Type B standard uncertainty associated with the neutral axis measurand can be determined using:

$$\delta y_0^B = \frac{2\beta |\varepsilon_b \varepsilon_t| h}{(\varepsilon_b - \varepsilon_t)^2} = \frac{2\beta |c|h}{(1-c)^2} \quad (3)$$

The combined standard uncertainty in the neutral axis determination, considering both the Type A and Type B standard uncertainties, can then be determined as:

$$\delta y_{0,c} = \sqrt{(\delta y_0^A)^2 + (\delta y_0^B)^2} \quad (4)$$

2.2 Distribution factor

In addition to changes in neutral axis locations, changes in distribution factors associated with specific lane loadings have also been proposed for the detection of structural damage in bridge spans. In practical application, distribution factors are computed from strains recorded along a transverse cross-section of the bridge with gages placed at the same location of each girder, often at the bottom flange

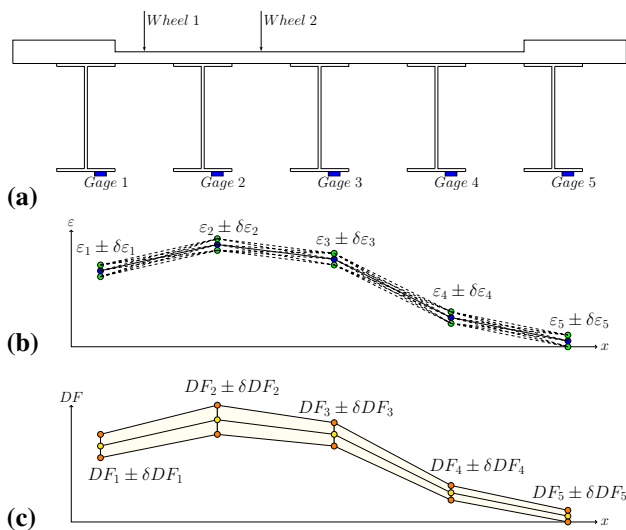


Fig. 3 Typical distribution factor measurement using an array of strain transducers across each girder of the superstructure. **a** Gage placement in the cross-section; **b** relative strain magnitudes across girders under vehicle load positioning; **c** effect of measurement uncertainties on accuracy of distribution factor determinations

(Fig. 3a). To develop an estimate of the distribution factor for each girder, the measured normal strain on the girder of interest, ε_i , is divided by the summation of the measured normal strains across all girders [13], as shown in the equation below:

$$DF_i = \frac{\varepsilon_i}{\sum_{j=1}^N \varepsilon_j} \quad (5)$$

where N is the number of girders in the cross-section.

As with neutral axis measurements, measurement uncertainties associated with the individual strain measurements (Fig. 3b) propagate through the calculation of the individual girder distribution factors and affect the confidence in the developed estimates (Fig. 3c). However, in contrast to the neutral axis measurement, uncertainty estimates for experimentally determined distribution factors have yet to be developed in prior literature. In this paper, the propagation formula [14] is applied to the distribution factor formula to produce

$$\delta DF_i = \frac{|\varepsilon_i + \sum_{j=1}^N \varepsilon_j|}{\left(\sum_{j=1}^N \varepsilon_j\right)^2} \delta \varepsilon_i + \sum_{j \in S} \left[\frac{|\varepsilon_i|}{\left(\sum_{j=1}^N \varepsilon_j\right)^2} \delta \varepsilon_j \right] \quad (6)$$

where S is the set formed by $\{j = 1 : N\} \cap \{j = i\}$. In other words, all summations over the set S are simply the sum of terms developed for $j \neq i$, where i is the girder of interest.

Under the assumption that the uncertainty in the measured strain is the same for all measurements, which is commonly valid for estimates developed from the experimental standard deviation of the mean, the Type A standard uncertainty estimate can be determined using:

$$\delta DF_i^A = \frac{(N-1)|\varepsilon_i| + \left|\sum_{j \in S} \varepsilon_j\right|}{\left(\sum_{j=1}^N \varepsilon_j\right)^2} \sigma(\varepsilon) \quad (7)$$

In addition, under the commonly encountered conditions that produce only positive (tensile) strains in the bottom flange of all girders, this equation can be further reduced, using the definition of the distribution factor, to yield:

$$\delta DF_i^A = \frac{1 + (N-2)DF_i}{\sum_{j=1}^N \varepsilon_j} \sigma(\varepsilon) \quad (8)$$

However, when transducer accuracy is considered within Type B evaluation of standard uncertainty using the model $\delta \varepsilon_k = \beta \varepsilon_k$, the following equation is developed from Eq. 6:

$$\delta DF_i^B = \frac{\left|\sum_{j \in S} \varepsilon_j\right| + \sum_{j \in S} |\varepsilon_j|}{\left(\sum_{j=1}^N \varepsilon_j\right)^2} \beta |\varepsilon_i| \quad (9)$$

Again, under the commonly encountered conditions that produce only positive (tensile) strains in the bottom flange

of all girders, this Type B standard uncertainty estimate can be further reduced to:

$$\delta DF_i^B = \frac{2 - 2DF_i}{\sum_{j=1}^N \varepsilon_j} \beta |\varepsilon_i| \quad (10)$$

As in the uncertainty evaluation for the neutral axis determination, the combined standard uncertainty in the distribution factor measurand, due to both Type A standard uncertainty related to the measurement precision and Type B standard uncertainty related to the transducer accuracy, can be determined using:

$$\delta DF_{i,c} = \sqrt{(\delta DF_i^A)^2 + (\delta DF_i^B)^2}. \quad (11)$$

2.3 Additional uncertainties

The derived equations and subsequent analysis examine the uncertainty in neutral axis and distribution factor estimates arising solely from transducer accuracy and resolution considerations. In the derivation of the neutral axis uncertainty formula (Eq. 1), the contribution of errors in the measurement of the transducer spacing, h , were not considered, nor were errors associated with the measurement of the gage locations relative to the datum of the cross-section [6]. Furthermore, while not considered in the development of the uncertainty formulae, uncertainties related to load positioning may contribute significantly to additional error in both the estimates of neutral axis locations and distribution factors. Distribution factors are by definition dependent on the load positioning and, while assumptions used in elementary mechanics often lead one to mistakenly believe that neutral axis locations are fixed to the centroid location, the actual apparent neutral axis location is dependent on the normal strain distribution produced by axial and bending response, which is dependent on the positioning of the loads. Significant additional uncertainties not explicitly considered in the uncertainty formula for neutral axis determination can be attributed primarily to the effects of biaxial bending [6] and shear lag phenomenon [15] on the distribution of normal strain in the cross-section. These effects may be important to consider when interpreting the apparent neutral axis as an indicator of damage, particularly if the damage present significantly affects the transverse stiffness of the cross-section. Lastly, strain transducers measure total strains, which include temperature-induced strains. With short-term strain measurements, the temperature-induced strains can be readily nulled from the recorded measurement signals to attenuate the direct effects of non-mechanical strains on the neutral axis and distribution factor measurements. However, if the elastic modulus of any of the materials in the composite cross-section is temperature-dependent, the neutral axis

locations and distribution factors will be affected by the temperature change.

3 Summary of experimental case study

3.1 Bridge description

To investigate the influence of measurement uncertainty on damage detection using strain-based measurements of changes in neutral axis and distribution factors, a real-world case study is leveraged using the experimental results in parallel with numerical predictions. The highway bridge investigated was a conventional concrete deck on steel girder superstructure design, which is a representative design type for a significant portion of the National Bridge Inventory. In fact, multi-girder/stringer bridge superstructures comprise nearly 42 % of the highway bridges in the United States and, furthermore, 55 % of the nearly 68,000 bridges that are structurally deficient in the US are of this design type [16]. The bridge was a two-lane structure consisting of a 13.7-m (45 ft) simply supported span. The bridge consisted of a 19.1-cm-thick reinforced concrete deck slab supported by three interior W840 × 226 (W33 × 152) and two W840 × 210 (W33 × 141) exterior steel girders. The girders had a uniform center-to-center spacing of 2.1 m (7 ft) and were supported by pin and rocker steel bearings. End diaphragms and intermediate diaphragms placed at the midspan were constructed of C380 × 50.4 (C15 × 33.9) sections that were bolted to transverse plates welded to the girders. A photograph of the bridge span with the truck used for controlled load application during the study is provided in Fig. 4 and the framing plan of the bridge design is presented in Fig. 5a. Prior to the scheduled closure for replacement, the structure serviced New York State Route 345 over Big Sucker Brook in the town of Waddington. Constructed in 1957, the bridge maintained a sufficiency rating of 61.2 % and an operational rating of 44.5 metric tons. At the time of the experimental testing,



Fig. 4 Photograph of instrumented bridge span and vehicle used for controlled application of test loads

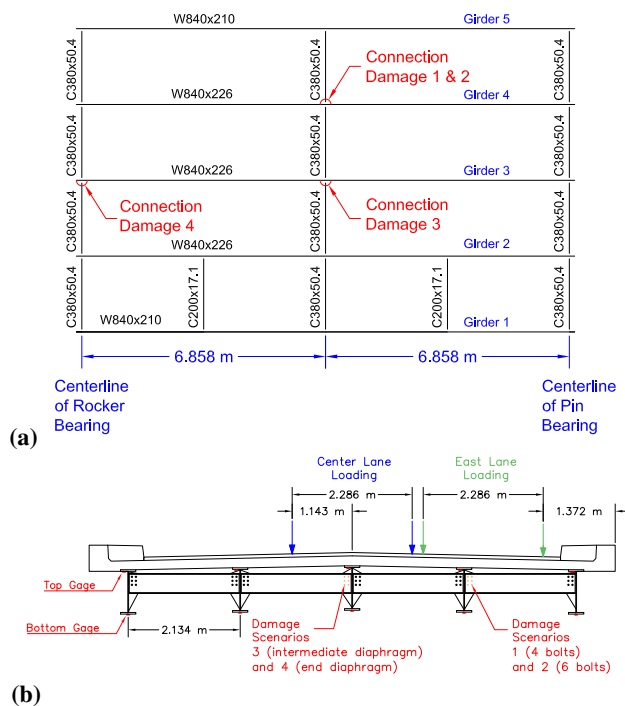


Fig. 5 **a** Framing plan of structure with locations of prescribed damages denoted; **b** cross-section of the superstructure showing the locations of the BDI strain transducers, prescribed damage scenarios, and truck lanes

the bridge was “R Posted” by New York State, indicating the “bridge does not have reserve capacity to accommodate most vehicles over legal weights, but can still safely carry legal weights”.

3.2 Instrumentation and testing protocol

Bridge Diagnostic Incorporated (BDI) strain transducers were deployed for completion of full-scale, controlled progressive damage tests of the bridge. These transducers feature a full Wheatstone bridge design for temperature compensation and are individually calibrated to NIST standards with a specified accuracy of less than $\pm 1\%$. The BDI transducers were installed at the top and bottom flanges of the steel girders at the midspan of the bridge. The cross-section of the bridge at the midspan is presented in Fig. 5b with the locations of the ten midspan strain transducers identified with red rectangles at the flange locations instrumented.

During the experimental test program, the bridge was subjected to prescribed vehicular lane loading applied by a NYSDOT transport truck estimated to weigh approximately 4.54 metric ton (5 ton) operating at crawl speeds. For the test program, the bridge was divided into three lanes (east, center, and west) although a construction barrier at the end of the span precluded reliable collection

of data from the west lane. The axle positions associated with the remaining lane loads is presented in Fig. 5b. As part of the study, several incremental levels of damage were applied to select girder-to-diaphragm connections by removing bolts from the connections to alter the load transfer within the structure. Locations of all affected connections are presented on the framing plan in Fig. 5a and identified in the cross-section in Fig. 5b. The damage scenarios presented in this paper began with removal of four bolts from the girder-to-diaphragm connection at girder four for the intermediate diaphragm spanning between the fourth and fifth girders. The second damage scenario incrementally advances the severity of this damage through removal of the remaining two bolts at the same connection. Following this damage case, another pair of progressive damage scenarios was introduced, but this time to the diaphragms spanning between the second and third girders. In the third damage scenario, all six bolts were removed from the girder-to-diaphragm connection for the midspan diaphragm at the connection to the third girder. Lastly, in the fourth and final damage scenario, all six bolts were removed from the girder-to-diaphragm connection for the northern end diaphragm at the connection to the third girder.

All damage scenarios introduced to the structure were progressive in nature to the prior damage scenarios; in other words, the damage introduced to the first girder-to-diaphragm connection was still present during the introduction of the third damage scenario and, likewise, for the fourth damage scenario. Photographs of the girder-to-diaphragm connection and removal of bolts at the connections are provided in Fig. 6. Further details on the introduced damage, including the effects of the prescribed damage on the ambient vibration response of the bridge and vibration-based damage detection results can be found in Whelan and Janoyan [17]. Neutral axis and girder distribution factor measurements were acquired for each girder over the sequence of lane loadings applied prior to the introduction of damage to establish baseline measurements and then following application of each damage scenario. All measures were obtained by first passing the measurement data through a 100-point moving average filter to attenuate any dynamic strains induced during the vehicle pass. Average strains were then computed over a 0.25-s time window centered about the peak measured strain recorded during the vehicle pass. Additional information pertaining to the instrumentation layout and testing protocols for both tests can be found in Gangone et al. [18].

In the experimental test program, signal conditioning for the BDI strain transducers was provided by National Instruments SCXI-1121 Isolation Amplifiers with 5 V excitation. Transducer signals were sampled at 10 kHz per channel using a National Instruments 16-bit PCI-6036E

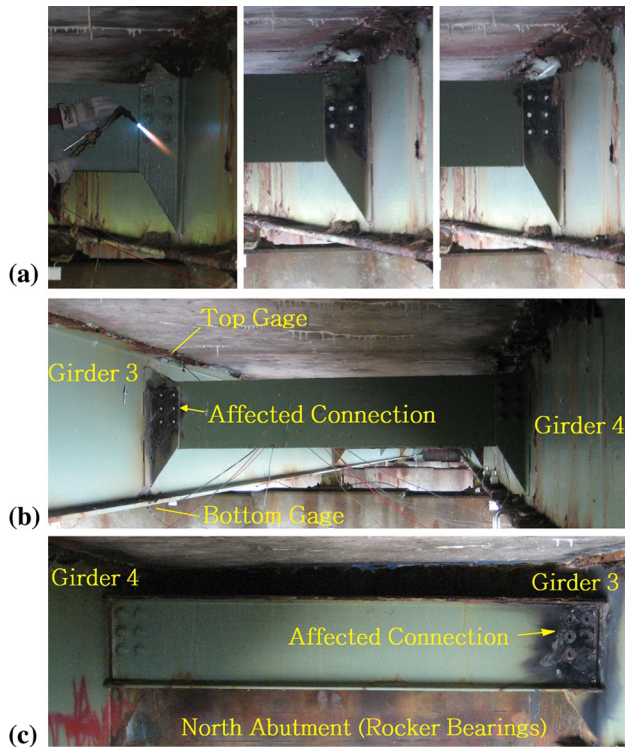


Fig. 6 Photographs of progressive damage: **a** introduced to intermediate diaphragm connection in damage scenarios 1 and 2; **b** damage scenario 3 (looking South); **c** damage scenario 4 (looking North)

Multifunction data acquisition card with 16-bit analog-to-digital converter. The digital signals were then passed through a digital decimation filter to reduce the effective sampling rate to 40 Hz. Analysis of the transducer outputs recorded during a period when the bridge was not loaded by traffic revealed an average peak noise level in the strain measurements to be $0.24 \mu\epsilon$, while the average standard deviation of the noise was approximately $0.10 \mu\epsilon$. Consequently, for this study the experimental standard deviation of the mean, $\sigma(\epsilon)$, was taken as $\pm 0.10 \mu\epsilon$. Given the specified transducer accuracy of $\pm 1\%$, the β used in this study was taken to be 0.01.

4 Finite element model used for comparison

A finite element model of the as-built design was developed in the SAP2000 v15 environment (Fig. 7). To provide reasonably faithful reconstruction of the prescribed damage scenarios, the girders, diaphragms, and diaphragm connection plates were modeled using shell elements rather than simplified beam elements. Individual bolts forming the connections between the web of the diaphragm members and the connecting plate were modeled with link elements prescribing shared translational degrees of freedom, but independent rotational degrees of freedom.

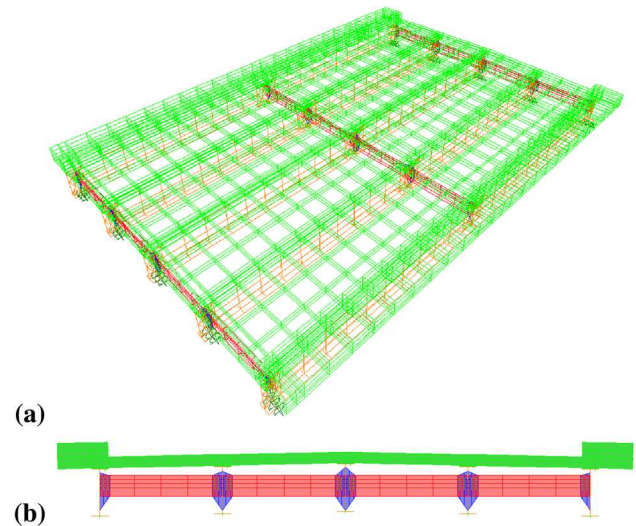


Fig. 7 Finite element model of the span

Simulation of the prescribed damage scenarios was then permitted by simply removing individual link elements from the model. To best capture localized tensile stresses around the point of load application commonly observed in experimental strain measurements at the top flange of the girders, the concrete deck was modeled using 8-node solid elements. Likewise, the haunches and curb of the bridge were modeled using solid elements. To facilitate data extraction from the model for correlation with the experimental measurements, strain transducers were explicitly modeled using short frame elements with moment and torsion releases. The bearing conditions for the bridge span were idealized using pin and roller boundary conditions at each end of the girders, respectively. In total, the finite element model was comprised of 2268 solid elements, 2444 shell elements, 330 frame elements, and 164 link elements.

To verify the predictive capability of the model prior to analysis, the linear modal parameters of the finite element model were compared to in-service estimates of natural frequencies and mode shapes of the bridge obtained through operational modal analysis. Ambient vibration monitoring was performed on the span throughout the experimental test program using the wireless sensor network described in Whelan and Janoyan [19]. The instrumentation for this monitoring consisted of 30 biaxial accelerometers mounted uniformly across the five girders of the structure and the response measurements were sampled in real time using an effective sampling rate of 128 Hz. Additional information on the ambient vibration monitoring for the structure can be found in Whelan and Janoyan [17]. The stochastic subspace state-space system identification algorithm described in Whelan and Janoyan [20] was used to develop estimates of the in-service modal

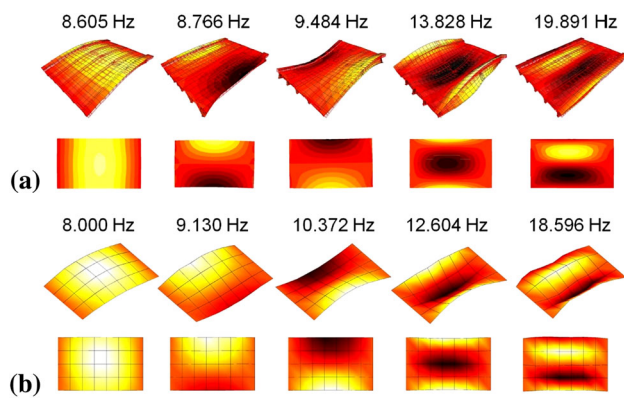


Fig. 8 Model verification: comparison of modal parameters of the finite element model to experimentally obtained estimates for the first five modes: **a** finite element model; **b** operational modal analysis

parameters. A comparison between the first five modes of the structure with the corresponding natural frequencies is presented in Fig. 8. Since all percentage errors in natural frequency estimates are below 10 %, the authors deem the correlation between the properties of the finite element model and the experimentally measured modal parameters to be reasonably strong given the difficulty of modeling a structure at the end of its service life.

Following this verification of the model, finite element analyses were performed to develop numerical influence lines for the axial strains developed at the transducer locations for each of the truck passes. The axle loads and spacing used in the experimental test program were then used to compute the expected strains in the structure for the baseline and progressive damage scenarios. All numerical results were processed using equivalent routines to those applied on the experimental data. Both neutral axis locations and distribution factors were computed from the finite element simulations for the case where the rear axle loads are positioned directly over the midspan of the bridge. This positioning corresponds to the peak strain measurement utilized in the experimental tests. The experimentally measured strains used for the following analysis are presented in Table 1, while those predicted by the finite element simulations and used are presented in Table 2.

5 Strain-based diagnostic results

To improve the clarity of the results presented, the damage scenarios are grouped into two categories of progressive damage. The first pair of scenarios presents a progressive deterioration of the load transfer mechanism between girders four and five by partial and then full removal of one of the bolted connections of the midspan diaphragm between these two girders. The second pair of scenarios presents a progressive deterioration of the load transfer

mechanism between girders two and three by complete removal of one of the bolted connections of the midspan diaphragm followed by the one of the end diaphragms between these two girders. By presenting these progressive scenarios independently, the results can be more easily interpreted to draw empirical conclusions on the performance of the diagnostic measures. Specifically, the data presented are reviewed to examine the sensitivity to damage of each measure relative to measurement uncertainties, consistency and progression of the diagnostic measures with severity of damage, and ability of the diagnostic to locate the source of the introduced damage.

5.1 Damage scenarios 1 and 2

In this section, changes in strain diagnostic indicators are presented only for damage scenarios 1 and 2, which correspond to two levels of damage severity at the same girder-to-diaphragm connection. During this stage of the analysis, the reference neutral axis locations and reference distribution factors for each lane loading are taken as those measured in the baseline state prior to the introduction of any intentional damage to the structure. In all cases, measurement uncertainties were calculated using Eqs. (2–4) for the neutral axis determinations and Eqs. (7, 9, 11) for the distribution factor determinations. These uncertainties are presented as error bars on the following figures summarizing the results. Note specifically that the error bars presented for all bar plots illustrating the relative changes in either apparent neutral axis location or distribution factor include both the uncertainty on the specific damage scenario measurement as well as the uncertainty associated with the baseline measurement.

5.1.1 Apparent neutral axis locations

The apparent neutral axis locations calculated from the strains simulated in the baseline finite element model as well as the relative changes in neutral axis locations corresponding to the two levels of damage severity relative to this baseline are presented in Fig. 9a, c. These estimates correspond to the conditions developed under the east lane and center lane loading. In each case, the neutral axis estimates represent apparent neutral axis locations, which include the effects of biaxial loading and shear lag and are specific to the load pattern. Presented alongside these numerical predictions are the experimentally obtained estimates of the apparent neutral axis locations for the baseline condition as well as the relative changes induced following the progressive damage cases (Fig. 9b, d). Note that the magnitude of strain developed in girder one for the east lane loading was so small that the measurement uncertainty exceeded ± 10 cm. Plotting these highly uncertain apparent

Table 1 Experimental strain measurements ($\mu\epsilon$)

	Baseline		Damage 1		Damage 2		Damage 3		Damage 4	
	East	Center	East	Center	East	Center	East	Center	East	Center
Girder 1 top gage	-0.31	0.96	-0.45	0.79	-0.47	0.65	-0.23	-0.47	-0.17	-0.42
Girder 1 bottom gage	-0.04	4.42	-0.08	3.51	-0.24	3.61	0.03	3.60	0.08	3.49
Girder 2 top gage	-0.78	-1.62	-0.75	-1.52	-0.61	-1.60	-0.59	-1.32	-0.66	-1.28
Girder 2 bottom gage	4.11	12.84	4.16	11.47	3.87	11.70	3.54	13.28	3.78	13.17
Girder 3 top gage	-0.23	-4.04	-0.41	-3.72	-0.81	-4.01	-1.74	-6.85	-1.91	-7.77
Girder 3 bottom gage	17.21	24.98	16.79	24.86	16.57	25.23	18.71	30.68	19.63	30.51
Girder 4 top gage	-4.08	-4.92	-4.16	-4.35	-5.49	-5.46	-6.78	-3.24	-5.75	-3.85
Girder 4 bottom gage	19.70	13.17	19.25	14.33	20.55	14.42	21.40	13.03	21.80	12.68
Girder 5 top gage	-2.23	-1.62	-1.66	-1.37	0.10	-0.10	-0.07	-0.08	-0.11	-0.07
Girder 5 bottom gage	16.42	3.73	15.52	4.33	16.77	4.21	15.30	3.10	14.83	3.00

Table 2 Finite element model strain predictions ($\mu\epsilon$)

	Baseline		Damage 1		Damage 2		Damage 3		Damage 4	
	East	Center	East	Center	East	Center	East	Center	East	Center
Girder 1 top gage	0.26	0.37	0.24	0.36	0.21	0.34	0.34	-0.01	0.32	-0.01
Girder 1 bottom gage	1.40	5.40	1.37	5.38	1.31	5.34	1.40	4.98	1.30	4.98
Girder 2 top gage	-0.54	-0.65	-0.56	-0.67	-0.60	-0.69	-0.58	-1.10	-0.59	-1.10
Girder 2 bottom gage	4.11	14.00	4.08	13.97	4.04	13.95	3.66	14.19	3.61	14.19
Girder 3 top gage	-1.39	-1.80	-1.45	-1.83	-1.52	-1.88	-1.53	-1.83	-1.52	-1.83
Girder 3 bottom gage	12.07	23.18	12.04	23.15	12.05	23.18	12.18	24.42	12.18	24.42
Girder 4 top gage	-0.71	-1.71	-0.65	-1.67	-0.80	-1.77	-0.81	-1.58	-0.80	-1.58
Girder 4 bottom gage	21.72	14.21	22.15	14.47	22.53	14.72	22.58	14.29	22.65	14.31
Girder 5 top gage	0.67	-0.18	0.67	-0.18	0.84	-0.10	0.84	-0.08	0.85	-0.08
Girder 5 bottom gage	20.67	5.33	20.47	5.22	20.44	5.17	20.44	4.88	20.49	4.87

neutral axis locations on the same figure as the remaining estimates would skew the scale of the graph to the extent that the response in the remaining girders with less uncertainty would no longer be visible. Consequently, the highly uncertain results obtained for this girder under the east lane loading are removed from this graph to improve the clarity of the figure.

While there are some differences in the baseline neutral axis locations relative to the finite element model predictions, these differences can be attributed to the advanced stage of existing deterioration in the actual structure that is not reflected in the model. Despite these initial differences between the baseline finite element model and the measured bridge response prior to the introduction of progressive damage, one might reason that the *relative* changes in bridge response due to the introduction of the controlled damage scenarios should be reflected reasonably consistently between the numerical model and the actual structure. However, significant differences are present between the relative changes predicted by the finite element

model and those measured experimentally. Specifically, the numerical model anticipates only relatively minor changes in apparent neutral axis locations that are generally within the uncertainty bounds associated with the measurement. This would suggest that the apparent neutral axis is not a reliable indicator of structural damage for this damage scenario in the presence of typical measurement uncertainty. However, the experimental results exhibit significant changes in apparent neutral axis locations typically outside the uncertainty bounds for girders adjacent to the location of the applied damage. While the magnitudes of the changes are significantly higher than predicted in the finite element model, the directions of apparent neutral axis location changes are often consistent with the model. Furthermore, the changes themselves seem to suggest the location of the prescribed damage through the clear increase in apparent neutral axis for girder five. In addition, the progression of damage severity is consistently observable in the relative changes measured in each girder across the two load cases.

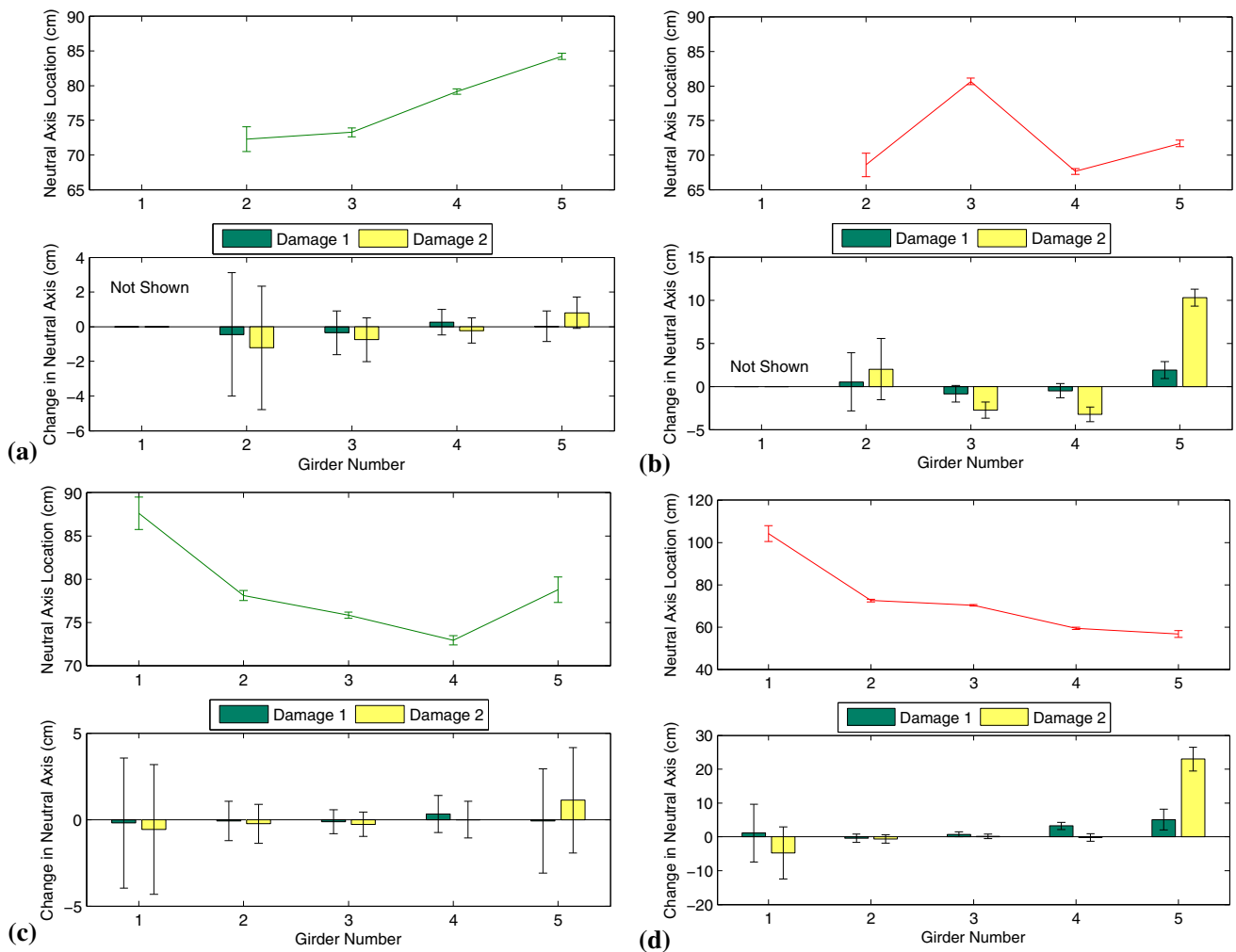


Fig. 9 Baseline apparent neutral axis locations and relative changes resulting from damage scenarios 1 and 2 shown with uncertainty bounds associated with $\sigma(\varepsilon) = 0.10 \mu\varepsilon$ and $\beta = 1 \%$: **a** finite element

simulations—east lane loading, **b** experimental data—east lane loading, **c** finite element simulations—center lane loading, **d** experimental data—center lane loading

In general, the experimental results support previously proposed use of the apparent neutral axis as a damage diagnostic indicator. However, the difference between the expected changes predicted by the finite element model and the experimental results should be particularly highlighted. The significant differences suggest that faithfully modeling the structural damage and its effect on apparent neutral axis locations, including the effects of biaxial bending and shear lag, is nontrivial. These effects are dependent on the extent of composite action in concrete deck on steel girder bridges and, in this case, the composite action was idealized as full. The discrepancies between experimental measurements and finite element predictions highlight the need for additional full-scale testing and verification of prior studies that have developed conclusions related to the use of neutral axis locations for damage detection based solely on numerical analyses.

5.1.2 Girder distribution factors

The baseline girder distribution factors for lane loading of the bridge, as predicted by the finite element model using the bottom strains at the midspan of the girders, are presented in Fig. 10a, c along with the predicted relative changes in girder distribution factors resulting from the prescribed damage. These simulated results indicate that changes in girder distribution factors are expected to occur at girders four and five for both the east and center lane loading across both damage scenarios. Due to the reduced load transfer between girders four and five resulting from the diaphragm connection damage, the model predicts that the distribution factor for girder four should increase for both lane loadings, while the remaining distribution factors decrease. However, the magnitude of these changes is just within the measurement uncertainty bounds, so the model

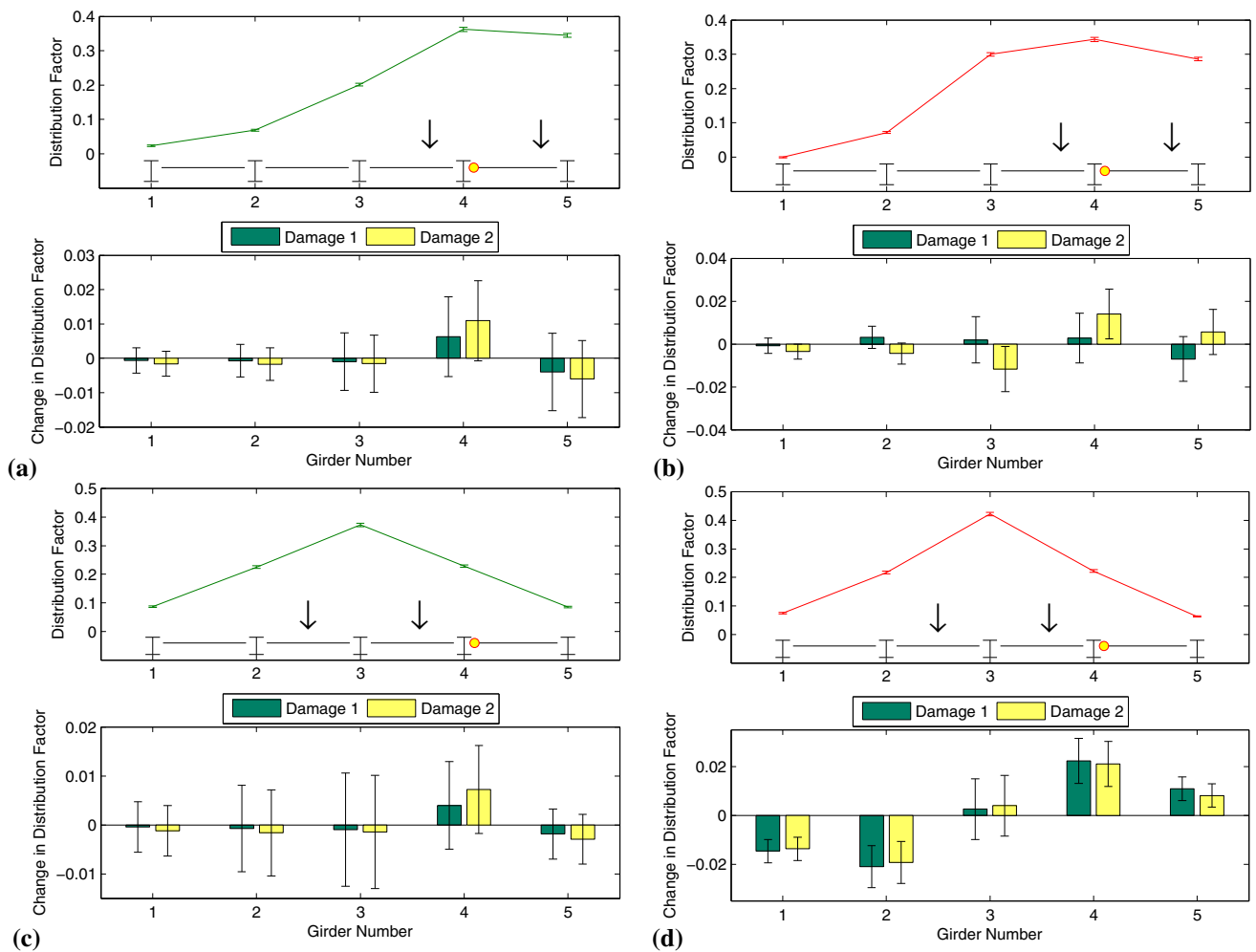


Fig. 10 Baseline girder distribution factors and relative changes for damage scenarios 1 and 2 shown with uncertainty bounds associated with $\sigma(\varepsilon) = 0.10 \mu\varepsilon$ and $\beta = 1\%$. **a** Finite element model—east lane

loading; **b** experiment—east lane loading; **c** finite element model—center lane loading; **d** experiment—center lane loading

suggest that distribution factors are not sensitive enough to the prescribed damage to exceed the uncertainties associated with conventional strain measurements.

Experimental measurements of the baseline distribution factors and relative changes during the first two damage scenarios are presented alongside the numerical data in Fig. 10b, d. The baseline girder distribution factors are more closely predicted by the finite element model than the apparent neutral axis locations, but also suggest that the finite element model over predicts the transverse stiffness of the cross-section. Experimental distribution factors predict an increase in distribution to girders four and five, where the affected diaphragm is located. While there are still discrepancies between the measurements and the model, the changes in experimental distribution factors are generally more consistent with those predicted by the finite element model than the corresponding apparent neutral axis location measurements. However, the experimental

data do not clearly demonstrate an ability to quantify the progression of the severity of damage from the first case to the second.

5.2 Damage scenarios 3 and 4

In this section, changes in strain diagnostic indicators are presented for damage scenarios 3 and 4, which correspond to midspan and then end diaphragm connection damage for the diaphragms between girders two and three (Fig. 5a). During this stage of the analysis, the reference neutral axis locations and reference distribution factors for each lane loading are taken as those measured after damage scenario 2. In all cases, measurement uncertainties were calculated using Eqs. (2–4) for the neutral axis determinations and Eqs. (7, 9, 11) for the distribution factor determinations. These uncertainties are presented as error bars on the following figures summarizing the results. Note specifically

that the error bars presented for all bar plots illustrating the relative changes in either apparent neutral axis location or distribution factor include both the uncertainty on the specific damage scenario measurement as well as the uncertainty associated with the reference measurement.

5.2.1 Apparent neutral axis locations

As for the prior cases, the reference apparent neutral axis locations and relative changes produced as a result of the prescribed damage are presented for the finite element analysis and experimental measurements in Fig. 11. For this series of prescribed damage scenarios, the finite element analysis again predicts changes in apparent neutral axis locations well below the measurement certainty for the east lane loading. In addition, while changes greater than the uncertainty bound are predicted in the model for the

center lane loading, the change is predicted to be most significant for girder one, which is not adjacent to the location of the damage. The experimental neutral axis measurements, while exceeding the uncertainty bounds for several girders, provide conflicting results in terms of identifying the location of the damage. Under the east lane loading, large decreases are measured in girders three and four, while a significant decrease is measured for girder one during the center lane loading. Again, the experimentally measured changes in apparent neutral axis locations are nearly an order of magnitude greater than those predicted numerically. However, the experimental measurements are reasonably consistent across the two damage cases with many of the girders indicating a mild progression of deterioration from damage scenario 3 to 4. Although these results indicate that apparent neutral axis locations are sensitive to the specific damage introduced and may reflect

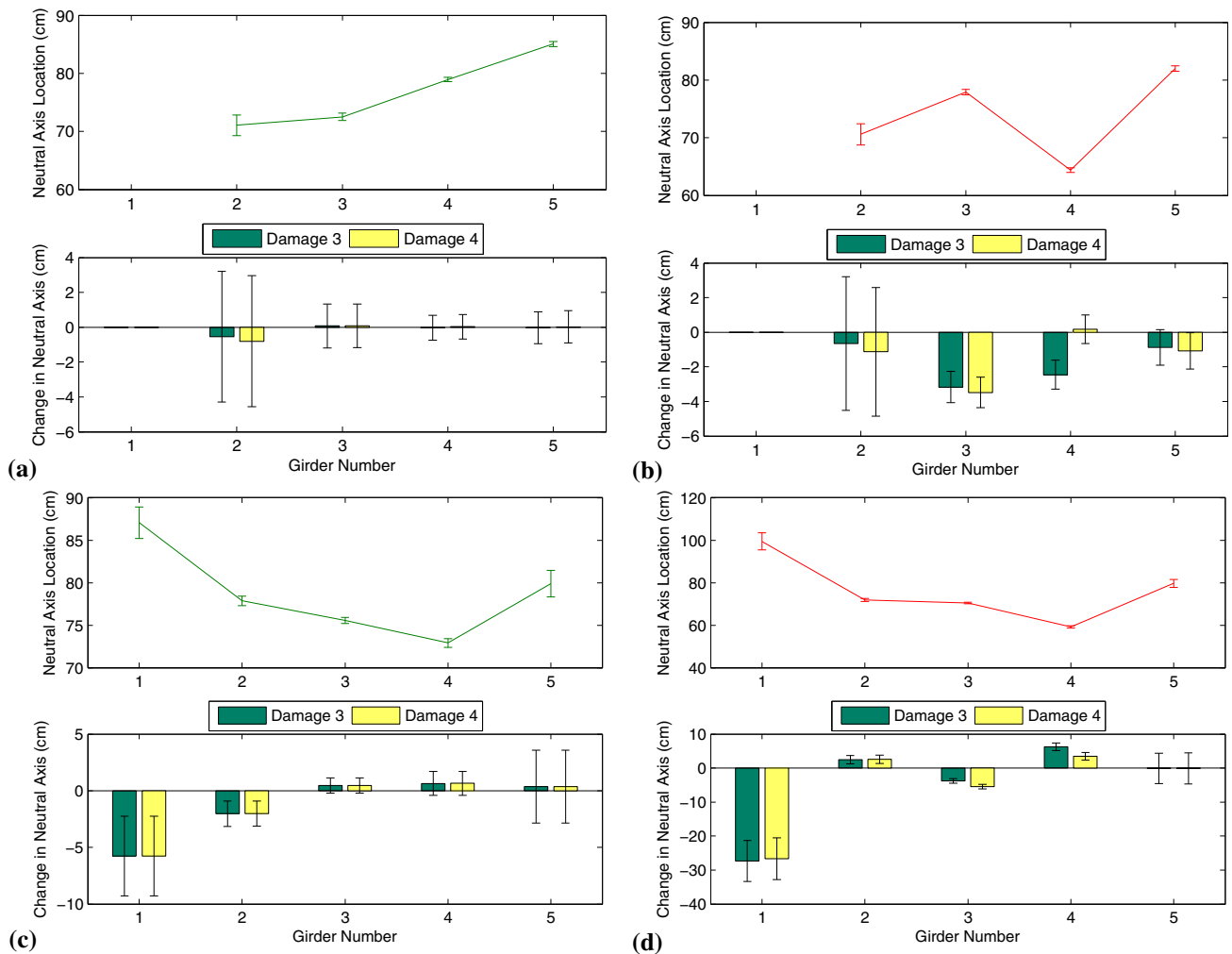


Fig. 11 Reference apparent neutral axis locations and relative changes resulting from damage scenarios 3 and 4 shown with uncertainty bounds associated with $\sigma(\epsilon) = 0.10\mu\epsilon$ and $\beta = 1\%$:

a finite element simulations—east lane loading, **b** experimental data—east lane loading, **c** finite element simulations—center lane loading, **d** experimental data—center lane loading

the severity of the damage, they do strongly emphasize the challenges associated with using this measure to locate and diagnose the source of the damage to the structure.

5.2.2 Girder distribution factors

Reference distribution factors from damage scenario 2 are presented alongside relative changes developed over the final two damage scenarios in Fig. 12 for both the finite element simulations and experimental measurements. In contrast to the apparent neutral axis measurements, the results suggest that girder distribution factors provide the capability to identify, localize, and indicate the severity of the damage. In the finite element simulations, the damage is reflected as a significant decrease in load distribution to the second girder under the east lane loading, while a significant increase in load distribution is predicted for the

third girder under the center lane loading. However, experimentally, the most significant increase in load distribution was measured for girder three in both cases. The increase in load distribution to the girder where the diaphragm connection was damaged is expected since the diaphragm connection damage reduces load transfer between the second and third girder under both loading patterns. This increase in load distribution to the girder with the affected connection is consistent with results from the prior damage scenarios. Again, the differences between the finite element simulation and experimental results are attributed to initial errors in modeling the transverse stiffness of the bridge. For this sequence of damage, the girder distribution factors also exhibit consistent relative changes from the reference data with indication of mild progression of severity as the damage is introduced to the end diaphragm connection.

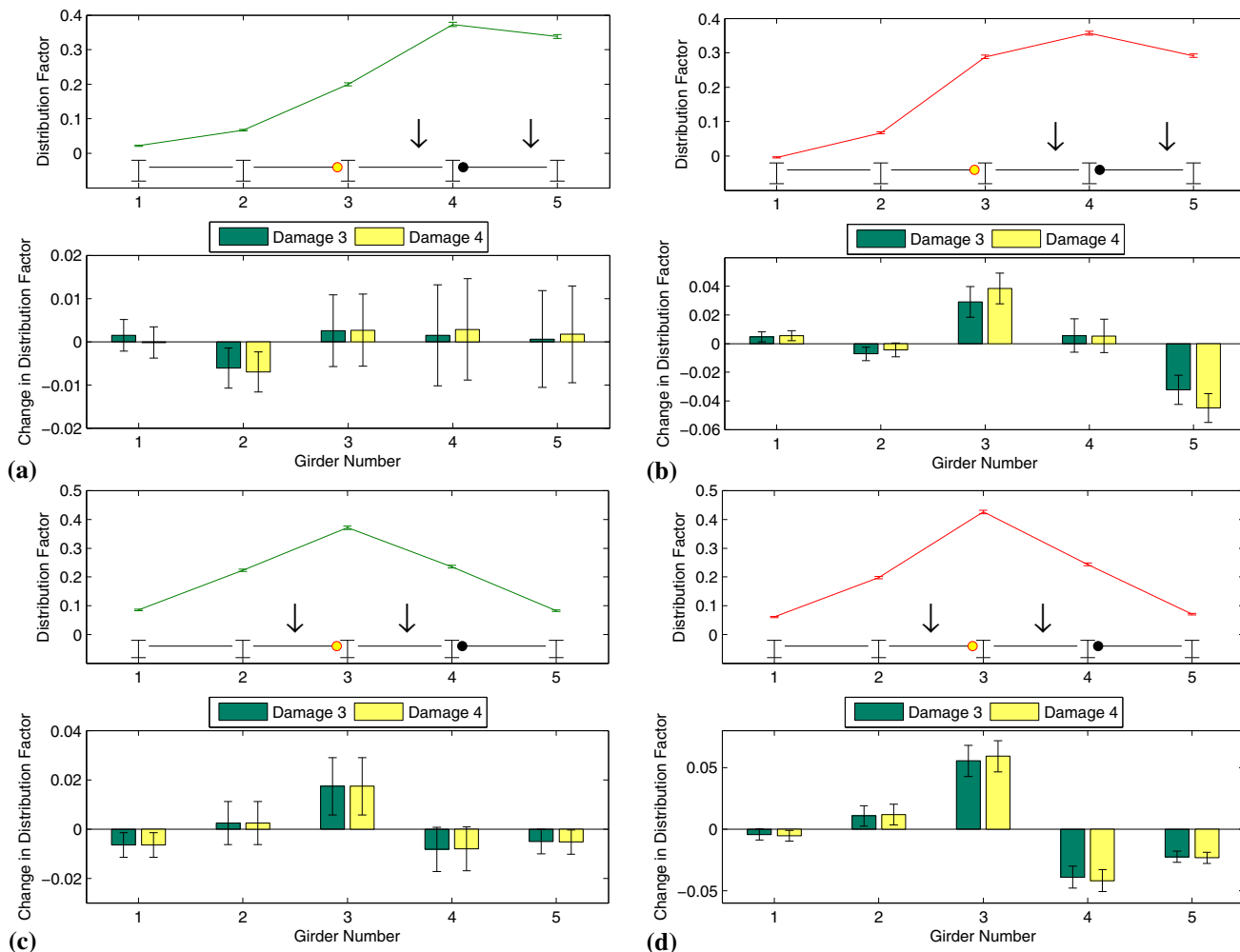


Fig. 12 Reference girder distribution factors and relative changes for damage scenarios 1 and 2 shown with uncertainty bounds associated with $\sigma(\epsilon) = 0.10 \mu\epsilon$ and $\beta = 1\%$. **a** Finite element model—east lane

loading; **b** experiment—east lane loading; **c** finite element model—center lane loading; **d** experiment—center lane loading

5.3 Summary of strain-based diagnostic results

In summary, experimental measurements of apparent neutral axis locations and girder distribution factors under two-lane loadings and across four damage scenarios suggest that both diagnostic measures exhibit sensitivity to the introduced diaphragm connection damage that exceeds the measurement uncertainty. Likewise, both measures exhibited generally consistent changes in their respective measures for each girder as the extent of damage to the load transfer mechanism between girders progressed. Furthermore, the progression of damage severity was generally exhibited in both measures as a mild amplification of the measured change. However, for these cases of diaphragm connection damage, the apparent neutral axis location was not able to reliably identify the location of the damage introduced to the structure directly. In contrast, experimental changes in girder distribution factors consistently exhibited their largest increase in load distribution to the girder where the diaphragm connection was damaged.

Comparisons of the experimentally measured changes in apparent neutral axis locations and girder distribution factors to those obtained through finite element simulations exhibit significant differences in predicted changes resulting from the prescribed damage. In all cases, the analytical model underestimated the measured changes, although the apparent neutral axis location measurements were most significantly under-predicted. Furthermore, in many cases, the finite element simulations predicted that the changes in apparent neutral axis locations would be within the measure of uncertainty, while the experimentally measured changes were often well outside the uncertainty. The comparisons emphasize the challenges associated with faithfully modeling structural damage and the effects on structural performance. In addition, these results suggest that previous conclusions regarding the use and performance of strain-based diagnostic measures based on finite element analysis require experimental validation. Lastly, the discrepancies emphasize the importance of continued full-scale structural health monitoring research on real structures subjected to quantifiable damage.

6 Conclusion

Numerous studies have proposed the use of strain-based measurement features for condition assessment of highway bridges, although only recently has the influence of measurement uncertainties been incorporated into experimental studies and applications. This paper has extended prior discussion of the transducer-based uncertainties on apparent neutral axis measurements and introduced formulae for girder distribution factor measurements. Experimental data

from a full-scale bridge case study with progressive structural damage applied to diaphragm connections were explored alongside a finite element model of the structure to examine the influence of uncertainties on relative changes to the apparent neutral axis and girder distribution factor measurements resulting from structural damage. The experimental study found that both apparent neutral axis locations and girder distribution factors were sensitive to the introduced damage beyond the calculated measurement uncertainty in all four cases analyzed. However, girder distribution factors were found to be more effective at identifying the location of the introduced damage. Specifically, the most significant changes in distribution factor were consistently observed as increases in load distribution to the girder where the diaphragm connection was affected. Lastly, significant discrepancies between predicted changes in diagnostic measures developed from the finite element model, particularly for apparent neutral axis locations, are highlighted in the analysis. These discrepancies challenge the use of analytical modeling as a means for developing and evaluating strain-based diagnostic approaches for structural health monitoring of highway bridges. Continued full-scale testing of structures subject to well-characterized damage is recommended to verify the performance of strain-based diagnostics under different mechanisms of structural damage and to validate conclusions previously developed based on numerical modeling.

Acknowledgments The authors would like to acknowledge the New York State Department of Transportation and, in particular, the Region 7 engineers and bridge maintenance crew for facilitating and assisting with the field testing.

References

1. Stallings J, Yoo C (1993) Tests and ratings of short-span steel bridges. *J Struct Eng* 119(7):2150–2168
2. Bakht B, Jaeger LG (1990) Bridge testing—a surprise everytime. *J Struct Eng* 116(5):1370–1383
3. Burdet OL (1993) Load testing and monitoring of Swiss bridges. Comité European du Béton, Safety and Performance Concepts, Lausanne, Switzerland
4. Pressley JS, Candy CCE, Walton BL, Sanjayan JG (2004) Destructive load testing of bridge No. 1049—analyses, predictions, and testing. In: Austroads 5th Bridge Conference, Hobart, Australia, May 1–12
5. Ni YQ, Xia HW, Ye XW (2012) Neutral-axis position based damage detection of bridge deck using strain measurement: numerical and experimental verification. In: 6th European workshop on structural health monitoring, Dresden, Germany, July 3–6
6. Sigurdardottir DH, Glisic B (2013) Neutral axis as damage sensitive feature. *Smart Mater Struct* 22(7):1–18
7. Plude S (2011) Implementing a long-term bridge monitoring strategy for a composite steel girder bridge. Master's Thesis, University of Connecticut
8. Kim S, Nowak AS (1997) Load distribution and impact factors for I-girder bridges. *J Bridge Eng* 2(3):97–104

9. Cardini AJ, DeWolf JT (2009) Long-Term structural health monitoring of a multi-girder steel composite bridge using strain data. *Struct Health Monit* 8(1):47–58
10. Reiff AJ (2014) Bridge structural health monitoring using statistical damage detection and advanced load rating methods. Masters of Science Thesis, Tufts University, Medford, MA, p 139
11. Joint Committee for Guides in Metrology (JCGM) (2008) Evaluation of measurement data—guide to the expression of uncertainty in measurement. Guide JCGM 100:2008
12. Glisic B, Inaudi D (2008) Fibre optic methods for structural health monitoring. Wiley, Chichester
13. Ghosn M, Moses F, Gobieski J (1986) Evaluation of steel bridges using in-service testing. *Transp Res Rec* 172:71–78
14. Rabinovich S (2005) Measurement errors and uncertainties: theory and practice. Springer, New York
15. Elhelbawey M, Fu CC, Sahin MA, Schelling DR (1999) Determination of slab participation from weigh-in-motion bridge testing. *J Bridge Eng* 4(3):165–173
16. Federal Highway Administration (2014) Tables of frequently requested NBI information. <http://www.fhwa.dot.gov/bridge/britab.cfm>. Accessed 30 Nov 2014
17. Whelan MJ, Janoyan KD (2010) In-service diagnostics of a highway bridge from a progressive damage case study. *J Bridge Eng* 15(5):597–607
18. Gangone MV, Whelan MJ, Janoyan KD, Minnetyan L (2013) Development of performance assessment tools for a highway bridge resulting from controlled progressive damage monitoring. *Struct Infrastruct Eng* 10(5):551–567
19. Whelan MJ, Janoyan KD (2009) Design of a robust. High-rate wireless sensor network for static and dynamic structural monitoring. *J Intell Mater Syst Struct* 20(7):849–863
20. Van Overschee P, DeMoor B (1996) Subspace identification for linear systems. Kluwer Academic Press, Boston